The c-Myc target gene *PRDX3* is required for mitochondrial homeostasis and neoplastic transformation

Diane R. Wonsey, Karen I. Zeller, and Chi V. Dang*

Program in Human Genetics and Molecular Biology and Department of Medicine, The Johns Hopkins University School of Medicine, Baltimore, MD 21205

Deregulated expression of the c-Myc transcription factor is found in a wide variety of human tumors. Because of this significant role in oncogenesis, considerable effort has been devoted to elucidating the molecular program initiated by deregulated *c-myc* expression. The primary transforming activity of Myc is thought to arise through transcriptional regulation of numerous target genes. Thus far, Myc target genes involved in mitochondrial function have not been characterized in depth. Here, we describe a nuclear c-Myc target gene, *PRDX3*, which encodes a mitochondrial protein of the peroxiredoxin gene family. Expression of *PRDX3* is induced by the mycER system and is reduced in *c-myc$^{-/-}$* cells. Chromatin immunoprecipitation analysis spanning the entire *PRDX3* genomic sequence reveals that Myc binds preferentially to a 930-bp region surrounding exon 1. We show that *PRDX3* is required for Myc-mediated proliferation, transformation, and apoptosis after glucose withdrawal. Results using mitochondria-specific fluorescent probes demonstrate that *PRDX3* is essential for maintaining mitochondrial mass and membrane potential in transformed rat and human cells. These data provide evidence that *PRDX3* is a c-Myc target gene that is required to maintain normal mitochondrial function.

The c-Myc transcription factor has been implicated in the control of a variety of cellular processes, including cell growth, cell-cycle progression, and apoptosis (1). The c-Myc protein is a member of the basic helix-loop-helix leucine zipper family of transcription factors. In cooperation with its heterodimerization partner Max, Myc binds DNA in a sequence-specific manner and activates transcription at E box elements with the consensus sequence 5′-CACGTG-3′. In an effort to dissect the molecular pathways regulated by Myc, several recent studies have focused on the use of microarray technology to identify the transcriptional targets of c-Myc (2–4). A coherent picture is beginning to emerge whereby Myc functions to accelerate multiple metabolic pathways, including amino acid and nucleotide synthesis, lipid metabolism, and glycolysis. Whether Myc also affects mitochondrial metabolism remains unclear. Because mitochondria play a central role in energy production as well as the execution of cell death, they represent a potential site for the regulation of both proliferation and apoptosis. Therefore, Myc target genes encoding mitochondrial proteins could play a significant role in tumorigenesis.

PRDX3 was first identified as a putative c-Myc target gene by using representational difference analysis (RDA) to identify genes that were differentially expressed between Rat1a (R1a) fibroblasts and R1a fibroblasts stably overexpressing c-Myc (R1a-*myc*) under conditions of anchorage-independent growth (5). Originally cloned as a gene expressed during the differentiation of murine erythroleukemia cells (6), *PRDX3* was subsequently shown to possess peroxide reductase activity (7). *PRDX3* belongs to an expanding family of highly conserved proteins termed peroxiredoxins, which catalyze the reduction of peroxides in the presence of thioredoxin (8, 9). Members of this gene family have been shown to be involved in diverse cellular roles, including proliferation (10), apoptosis (11), and the response to oxidative stress (12). The bovine *PRDX3* homolog, SP-22, localizes to mitochondria, and SP-22 expression is induced after exposure to peroxides or mitochondrial respiratory chain inhibitors (12). The potential role of *PRDX3* in tumorigenesis has recently been examined in breast cancer, where elevated levels of PRDX3 protein were found in 79% of the cases examined (13).

In our present study, we sought to determine whether *PRDX3* was a bona fide Myc target gene by using Northern analysis of *PRDX3* in several model systems. By using chromatin immunoprecipitation (ChIP), we also have examined the occupancy of Myc at multiple sites within the *PRDX3* genomic sequence during serum stimulation of 2091 primary human fibroblasts. Then, we evaluated whether *PRDX3* has a functional role in Myc-mediated cellular phenotypes. Deregulated c-*myc* expression induces cell-cycle progression (14), cellular proliferation, anchorage-independent growth (15), and apoptosis after withdrawal of serum (16) or glucose (17). In an effort to establish whether *PRDX3* expression affects Myc-induced transformation, we generated stable Rat1a-*myc* fibroblast cell lines expressing murine *PRDX3* in either the sense or antisense (AS) conformation. These cell lines then were evaluated in proliferation and apoptosis assays. To apply our findings to other cell systems, we chose the MCF7/ADR human breast cancer epithelial cell line (18) for further study of *PRDX3*. Our results demonstrate that c-Myc directly activates expression of a mitochondrial peroxiredoxin that is required for Myc-mediated transformation.

Materials and Methods

Northern Blotting. Northern blot analysis was performed as described (5). Blots were analyzed and quantitated on a PhosphorImager (Molecular Dynamics). The murine *PRDX3* cDNA probe was obtained from IMAGE clone 577524. For R1a and R1a-*myc* cells, RNA was collected from logarithmically growing cells (adherent) or from cells grown in suspension for 48 h over a layer 0.7% agarose in DMEM (nonadherent). The blot was hybridized simultaneously with probes for *PRDX3* and *rpL32* (5). For *in vivo* analysis of *PRDX3* expression, total RNA was isolated from mouse liver at 3, 4, and 5 days after adenoviral injection, as described (19). Twenty μg of RNA was loaded for each sample. Analysis of *PRDX3* expression in 2091 primary human fibroblasts was performed by placing 50% confluent 2091 cells (American Type Culture Collection) in media containing 0.1% serum. After 48 h, confluent cells were stimulated with DMEM containing 10% (vol/vol) serum, and RNA was collected at the indicated time points. Northern blots containing 10 μg of RNA

BIOCHEMISTRY

were probed with either human c-*myc* or *PRDX3*. The *PRDX3* and c-*myc* signals were normalized to the ethidium bromide-stained gel of 18S RNA, which was quantitated with LABWORKS image analysis software (Ultraviolet Products).

Chromatin Immunoprecipitation. Quiescent human primary 2091 fibroblasts were serum stimulated for 0 or 2 h. ChIP was performed with α-Myc antibody (Santa Cruz Biotechnology, sc-764), as described (20). For PCR, 1/100th of the immuno-precipitate was used. PCR primers are given in Table 1, which is published as supporting information on the PNAS web site, www.pnas.org, and were designed by using the human *PRDX3* genomic DNA sequence from the GenBank database (contig NT 008902). Real-time PCR was performed by using Sybr Green PCR core reagents (Applied Biosystems) according to the kit protocol (fragments D, F, G, I) or with $1\times$ PCR buffer (Invitrogen), 2.5 mM MgCl$_2$, 0.2 mM dNTPs, 1.25 units of Platinum *Taq* (Invitrogen), 0.5 μM primers, and $1\times$ Sybr Green buffer (fragments A, B, C, E, H). Absolute quantitation of Myc-bound chromatin was performed by comparing the cycle threshold of each ChIP product to a standard curve generated with known amounts of total-input genomic DNA. Each reaction was analyzed within the linear range, and reactions were performed in triplicate.

Plasmids. Murine *PRDX3* cDNA was obtained from IMAGE consortium clone 577524. pSG5-*PRDX3* and pSG5-*PRDX3*AS were created by cloning the Klenow-filled *Not*I-*Eco*RI fragment of 577524 into the Klenow-filled *Eco*RI site of pSG5 (Stratagene). Human *PRDX3* cDNA was obtained from IMAGE consortium clone 50888. pSG5-*PRDX3* and pSG5-*PRDX3*AS were created by *Not*I digestion of clone 50888 followed by partial digestion with *Hin*dIII. The 1.5-kb fragment corresponding to *PRDX3* was filled with Klenow and cloned into the blunt Klenow-filled *Eco*RI site of pSG5. Constructs were screened for orientation and sequenced.

Stable Transfectants. Stable pooled cell lines were generated by cotransfection of pSG5, pSG5-*PRDX3*, or pSG5-*PRDX3*AS with the puromycin resistance plasmid pBabe-puro (21) by using Lipofectamine (GIBCO) according to the manufacturer's instructions.

Immunoblotting. Immunoblotting was performed as described (5). Polyclonal rabbit antipeptide antibodies to murine PRDX3 were generated against amino acids 80–95 of murine PRDX3 (Research Genetics, Huntsville, AL). Polyclonal rabbit antipeptide antibodies to human PRDX3 were generated against amino acids 241–256 of human PRDX3 (Zymed). Monoclonal β-actin antibody was from Sigma (A-5441).

Growth and Transformation Assays. Growth curves were generated by plating triplicate samples for each cell line at an initial density of 5×10^3 cells per sample for R1a-*myc* cells or 1×10^4 cells per sample for MCF7/ADR cells. Live cells were counted by using a hemocytometer. The average cell number was plotted, curve fits were used to calculate doubling times, and R^2 values were greater than 0.97 in each case. Methylcellulose assays consisted of four 35-mm dishes per cell line, at a density of 2×10^3 cells per dish, plated in 1 ml of 1.3% methylcellulose in DMEM. Photomicrographs were taken after 8 days (pSG5 and *PRDX3*) or 16 days (*PRDX3*AS). Colonies of all sizes from two experiments were counted after 7 days (pSG5 and *PRDX3*) or 14 days (*PRDX3*AS) to adjust for differences in doubling time.

Nude Mouse Assays. Cells (5×10^6) in 200 μl of sterile PBS were injected s.c. into the right flank of male homozygous nude mice at 6 weeks of age. Tumors were allowed to establish until the estimated tumor mass exceeded 1,500 mg. Experiments were approved by the Johns Hopkins School of Medicine Animal Care and Use Committee.

Flow Cytometric Analyses. For apoptosis assays, cells were seeded at 5×10^5 per 10-cm^2 plate and exposed to either media containing 0.1% serum or glucose-free media for 24 h. Cells were collected and stained with 5 μg/ml propidium iodide and FITC-conjugated annexin V (BioSource International, Camarillo, CA), followed by analysis using a Coulter EPICS 752 flow cytometer. All annexin V positive cells were included for statistical analysis.

For fluorescence activated cell sorter (FACS) analysis of reactive oxygen species, mitochondrial membrane potential, and mitochondrial mass, cells were seeded at 5×10^5 per 10-cm^2 plate and incubated at 37°C in 5% CO$_2$ for 30 min in the presence of 5 mg/ml 2′,7′-dichlorodihydrofluorescein diacetate (DCFH-DA), 20 nM DiOC$_6$, or 100 nM NAO, respectively, all from Molecular Probes. Cells were washed with PBS, trypsinized, and resuspended. Cells incubated with DCFH-DA were resuspended in ice-cold media containing 5 mg/ml DCFH-DA and maintained on ice until analysis. Cells in DiOC$_6$ were resuspended in 37°C media and analyzed immediately. NAO-labeled cells were resuspended in 37°C media containing 100 nM NAO and analyzed immediately. All analyses were performed with a Becton-Dickinson FACScan flow cytometer with a 488-nm argon laser. All analyses were performed at least three times, and a representative histogram is shown.

Electron Microscopy. Adherent cells were embedded by using the Pelco Eponate 12 kit (Ted Pella, Inc., Redding, CA). Then, cells were sectioned, followed by staining with uranyl acetate and lead citrate. Analysis was performed by using transmission electron microscopy.

Results

Analysis of *PRDX3* Expression in Response to c-Myc. Northern analysis confirms the results of the original RDA screen, as shown in Fig. 1*A*. *PRDX3* is two-fold more highly expressed in adherent R1a-*myc* cells relative to R1a, with the difference in expression becoming six-fold when the cells are nonadherent. Because R1a cells growth-arrest when they are not attached to a substrate while R1a-*myc* cells continue to proliferate (5), the original RDA screen cannot distinguish between direct c-Myc target genes and genes that are growth-related, non-Myc targets. Therefore, we used the Rat1MycER system (14, 22) to determine whether Myc directly activates *PRDX3*. This system utilizes a fusion of c-*myc* to the hormone-binding domain of the estrogen receptor. The fusion protein is retained in the cytosol until the addition of tamoxifen, an estrogen analog, whereupon the protein translocates to the nucleus and activates its biological targets. Cycloheximide is used to inhibit protein synthesis, thereby allowing identification of genes that are directly activated by Myc. Fig. 5*A*, which is published as supporting information on the PNAS web site, shows that *PRDX3* expression increases in the presence of both cycloheximide and tamoxifen, suggesting that c-Myc directly activates transcription of *PRDX3*. Examination of logarithmically growing c-*myc*-null fibroblasts (23) indicates that *PRDX3* expression is decreased by 50% in the absence of *myc* (Fig. 1*B*). *PRDX3* expression is also induced during serum stimulation of quiescent c-*myc*$^{+/+}$ cells (Fig. 5 *B* and *C*). *PRDX3* expression increases after 1 h of serum stimulation and reaches a maximum of 2.8-fold after 16 h. However, only a 1.3-fold increase is seen after serum stimulation of c-*myc*$^{-/-}$ cells. These results indicate that *PRDX3* is a c-Myc responsive gene and that *PRDX3* expression is minimally induced by serum in the absence of Myc.

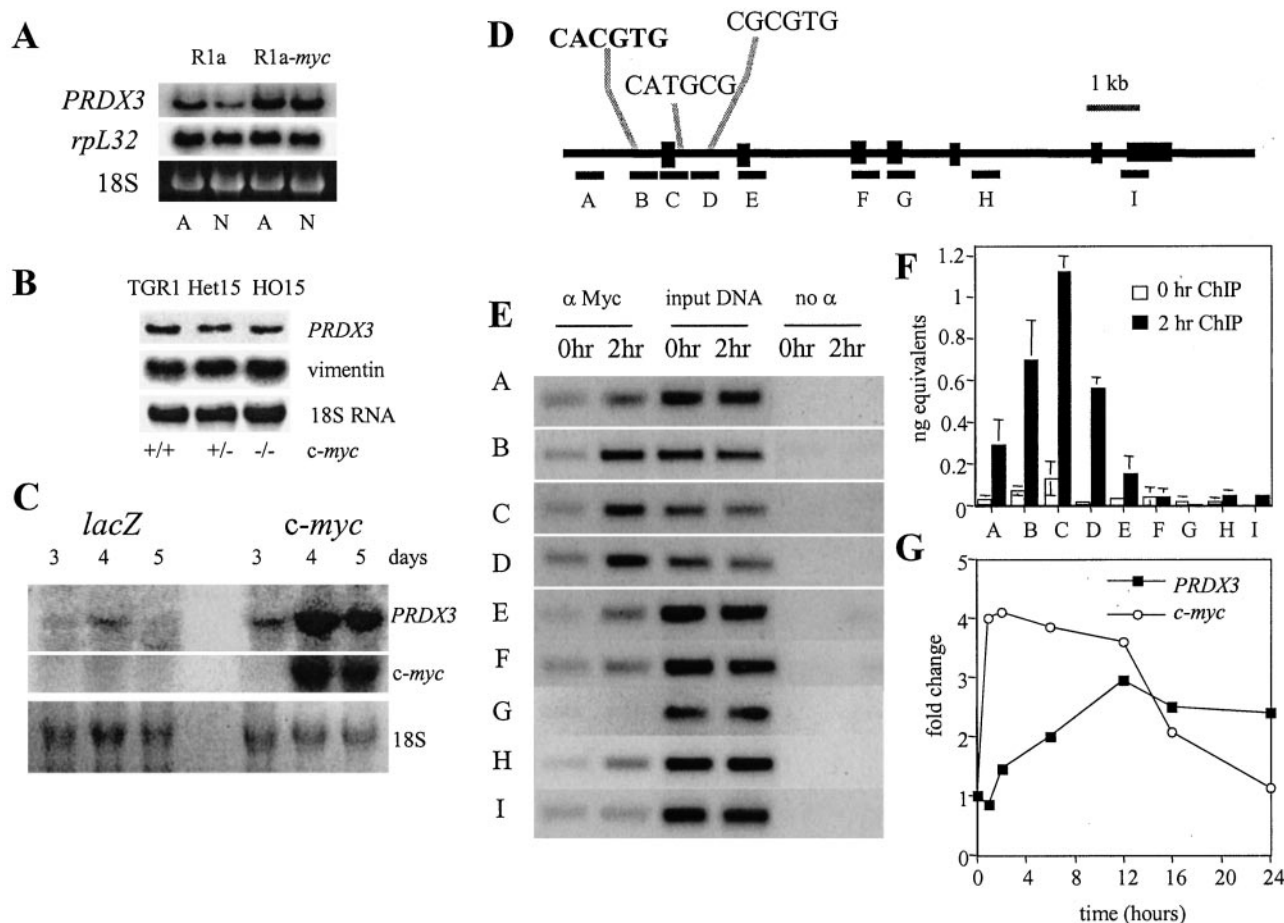A recently described *in vivo* model of transient c-Myc over-

Fig. 1. *PRDX3* is regulated by *c-myc* expression. (*A*) RNA from Rat1a (R1a) fibroblasts or Rat1a fibroblasts expressing ectopic c-Myc (R1a-*myc*). *rpL32* is shown as a loading control. RNA was isolated from adherent cells (A) or nonadherent cells grown over a layer of agar (N). (*B*) *PRDX3* expression in logarithmically growing c-*myc*^{+/+}, [+/−], or [−/−] Rat1 fibroblasts. *PRDX3* expression was calculated relative to vimentin. (*C*) Hepatic RNA from mice injected with either adenoviral *LacZ* or c-*myc*. Numbers represent days after injection with adenovirus. 18S RNA is shown as a loading control. (*D*) Schematic representation of the *PRDX3* genomic locus. Exons are indicated by black boxes. Fragments analyzed for Myc binding are indicated by lettered black bars. The sole canonical E box is indicated in bold, and noncanonical E boxes (38, 39) in fragments *C* and *D* are also shown. (*E*) Ethidium bromide-stained gels of PCR products. (*F*) Sybr green analysis of PCR fragments evaluated for Myc binding. The absolute amount of DNA in each sample was calculated, and the average was plotted ± SD. (*G*) Relative mRNA levels for c-*myc* and *PRDX3* during serum stimulation. Signals were normalized to the level of 18S RNA and plotted relative to the 0 h time point for each series.

expression (19) also indicates that c-Myc regulates *PRDX3*. Mice injected with adenoviral c-*myc* show a dramatic increase in hepatic *PRDX3* expression, whereas mice injected with control *LacZ* adenovirus show a minimal increase in *PRDX3* (Fig. 1*C*). The increase in *PRDX3* expression parallels that of c-*myc*. To determine whether Myc binds directly to *PRDX3 in vivo*, we performed chromatin immunoprecipitation during serum stimulation of primary human fibroblasts. Scanning analysis of the 11-kb genomic *PRDX3* sequence (Fig. 1*D*) indicates that Myc binds to a region containing the sole canonical E box 179 bp upstream from the translational start site, as well as two noncanonical E boxes within the first intron of *PRDX3* (Fig. 1*E*). Quantitative real-time PCR analysis of *PRDX3* when Myc levels are low, at 0 h, indicates that most fragments exhibit a similar level of binding (Fig. 1*F*, white bars). At 2 h, Myc binds fragments B, C, and D preferentially, with fragment C showing a 22-fold increase in binding relative to negative distal sites F, H, and I (Fig. 1*F*, black bars). Despite the presence of multiple noncanonical E boxes located throughout the genomic *PRDX3* sequence, Myc binds specifically within a 930-bp region, spanning fragments B, C, and D at the 5′ end of *PRDX3*. Northern blot analysis during serum stimulation of 2091 fibroblasts indicates that *myc* expression is maximal between 1–2 h (Fig. 1*G*).

Expression of *PRDX3* is induced after 2 h and reaches a maximum at 12 h. Taken together, our results establish that Myc binds directly to *PRDX3 in vivo* and activates transcription.

Effect of *PRDX3* on Proliferation and Apoptosis in Rat1a-*myc* Cells. To determine the role of *PRDX3* in Myc-mediated transformation, we generated pooled R1a-*myc* fibroblast cell lines stably expressing murine *PRDX3* in either the sense or AS conformation (Fig. 2*A*). Characterization of the growth rate of these cells shows a decrease in the growth rate of R1a-*myc-PRDX3*AS cells, whereas control and R1a-*myc-PRDX3* cells display similar doubling times (Fig. 2*B*). This decrease in growth rate is not caused by increased apoptosis, as staining with annexin V is nearly identical among the three cell lines (data not shown). Because *PRDX3* was originally identified in a screen under conditions of anchorage-independent growth, we hypothesized that *PRDX3* would affect colony formation in semisolid media. Fig. 2*C* demonstrates that R1a-*myc-PRDX3* cells form colonies at a higher frequency than pSG5 control cells, whereas cells with *PRDX3*AS form very few colonies. To determine whether our observations applied *in vivo*, we injected these same cells into nude mice (Fig. 2*D*). R1a-*myc* cells expressing AS *PRDX3* did not readily form tumors and were only slightly more tumorigenic than R1a cells expressing control
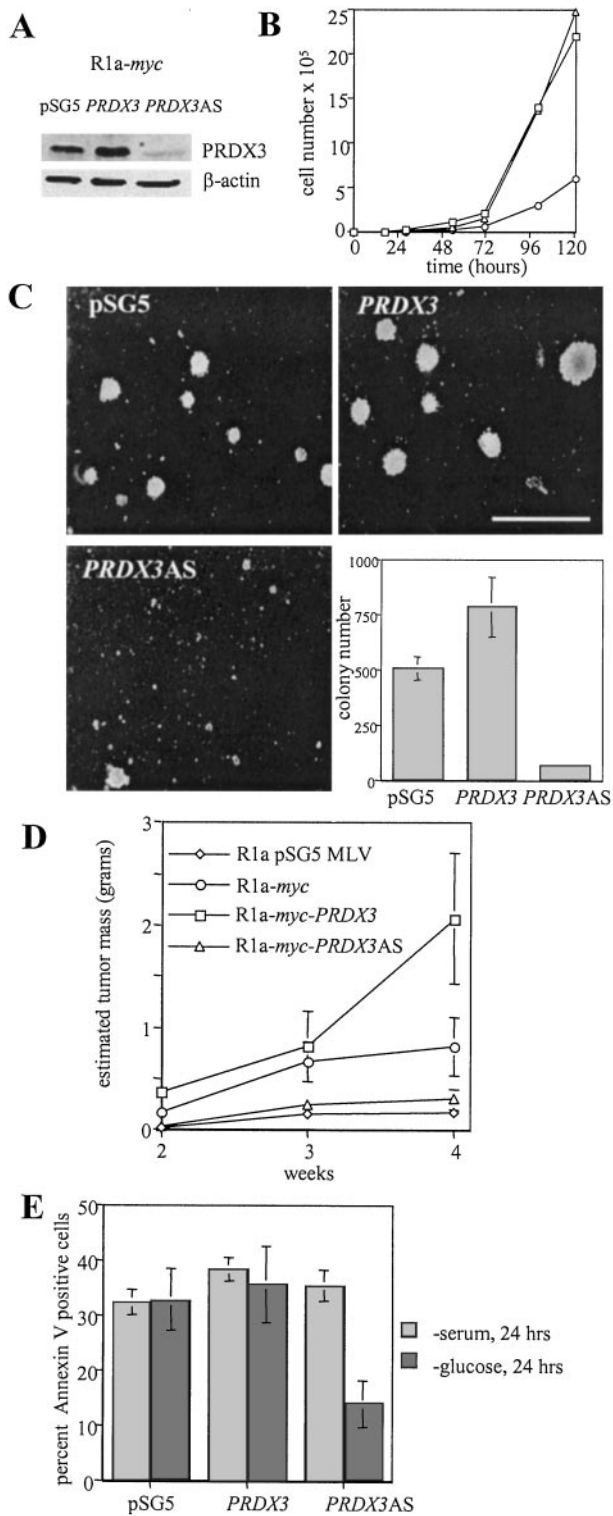
Fig. 2. Effect of *PRDX3* expression on doubling time, transformation, and apoptosis in R1a-*myc* cells. (*A*) Immunoblot analysis of cell lysates from R1a-*myc* cells transfected with pSG5 empty vector, pSG5-*PRDX3*, or pSG5-*PRDX3*AS. (*B*) Growth curves of R1a-*myc* transfectants: pSG5 (□), *PRDX3* (△), and *PRDX3*AS (○). Doubling times were 10.4, 10.9, and 19.0 h, respectively. (*C*) Photomicrographs of methylcellulose colonies. (Bar = 500 μM.) The bar graph represents the average colony number per 35-mm dish ± SD. (*E*) Tumor formation in nude mice. The average estimated tumor mass was plotted at 2, 3, and 4 weeks after injection ± SD (*n* = 8). (*D*) Percentage of apoptotic cells 24 h after serum deprivation (light bars) or glucose deprivation (dark bars). The average ± SD of three experiments is shown.
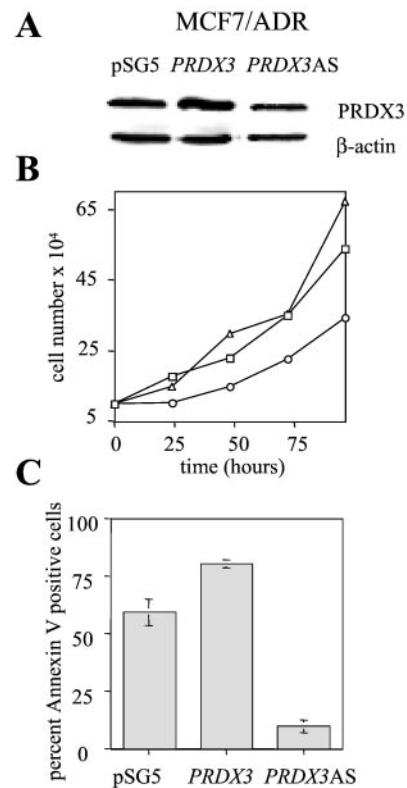
Fig. 3. Effect of *PRDX3* expression on doubling time and apoptosis in MCF7/ADR cells. (*A*) Immunoblot analysis of cells lysates from MCF7/ADR cells transfected with pSG5, pSG5-*PRDX3*, or pSG5-*PRDX3*AS. (*B*) Growth curves of MCF7/ADR transfectants: pSG5 (□), *PRDX3* (△), and *PRDX3*AS (○). Doubling times were 43.0, 37.6, and 60.2 h, respectively. (*C*) Percentage of apoptotic cells 24 h after glucose withdrawal. The average ± SD of three separate experiments is shown.

vectors alone (R1a pSG5 MLV). In contrast, R1a-*myc* cells overexpressing *PRDX3* formed larger tumors than R1a-*myc* cells, suggesting that elevated *PRDX3* expression confers a growth advantage *in vivo*. These results indicate that *PRDX3* affects both growth rate and transformation in R1a-*myc* cells. We also used these cell lines to examine Myc-induced apoptosis after serum or glucose deprivation. We found that *PRDX3* expression does not affect apoptosis after serum deprivation (Fig. 2*E*, light bars). However, *PRDX3* does affect apoptosis after glucose withdrawal (Fig. 2*E*, dark bars). Cells expressing AS *PRDX3* are resistant to apoptosis after removal of glucose, whereas cells with increased *PRDX3* remain sensitive to glucose deprivation-induced apoptosis.

Effect of *PRDX3* on Proliferation and Apoptosis in MCF7/ADR Cells. To demonstrate that our findings were not specific to R1a-*myc* cells, we chose the MCF7/ADR human breast cancer epithelial cell line (18). This cell line undergoes extensive apoptosis after glucose withdrawal, and apoptosis can be inhibited by reduction of c-Myc expression with AS oligonucleotides (24). Apoptosis depends on the formation of oxygen radicals, as inhibition of oxygen radical formation using the free radical scavenger sodium pyruvate is sufficient to inhibit apoptosis (25). By using full-length human *PRDX3* cDNA, we generated stable pooled cell lines that either overexpress or show decreased levels of human PRDX3 protein (Fig. 3*A*). Analysis of the growth rate of these cells shows that *PRDX3*AS cells show a decreased growth rate relative to control cells, although the result is less dramatic than that for R1a-*myc* cells (Fig. 3*B*). We also assayed apoptosis after
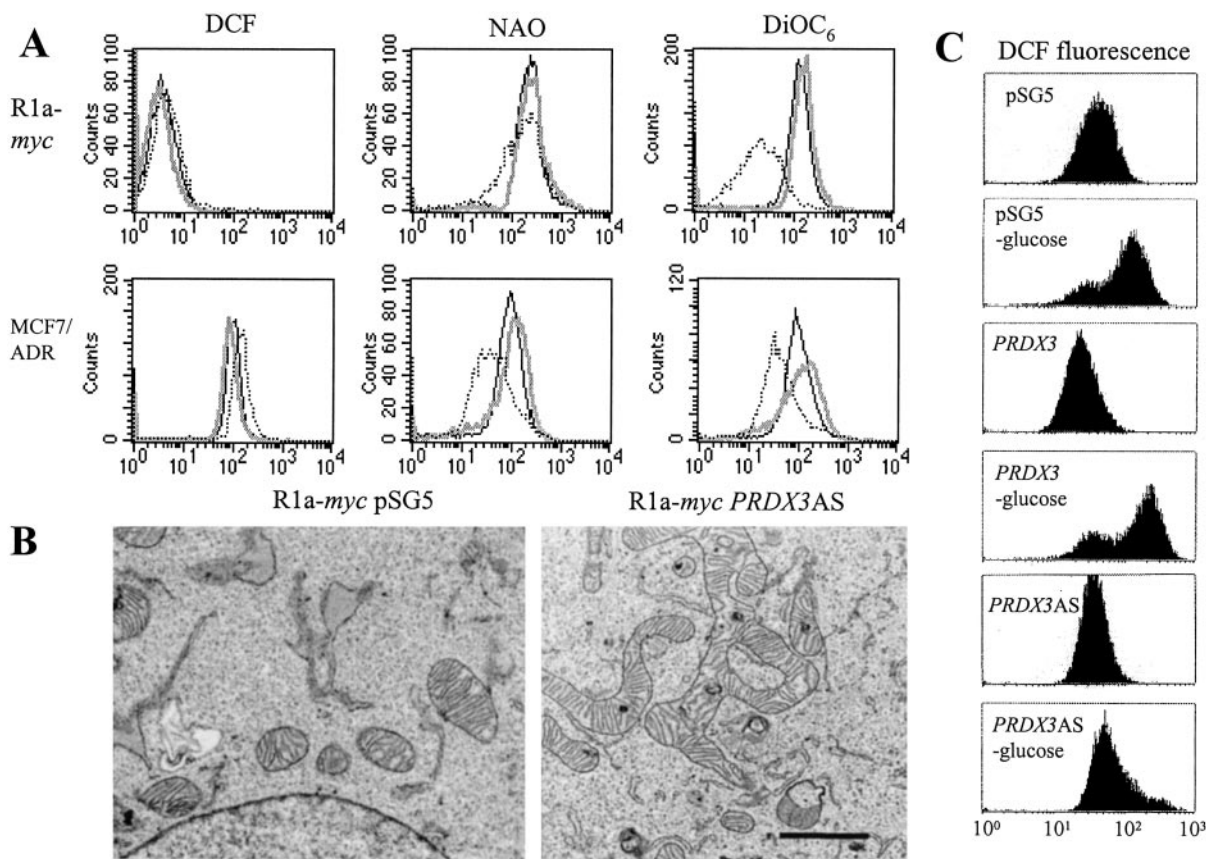
Fig. 4. *PRDX3* affects mitochondrial membrane integrity and morphology. (*A*) Histograms generated by FACS analysis of cells incubated with dye specific for cellular reactive oxygen species (DCF), mitochondrial mass (NAO), or mitochondrial membrane potential (DiOC$_6$): pSG5 (solid black line), *PRDX3* (solid gray line), *PRDX3*AS (dotted line). (*B*) Transmission electron microscopy of R1a-*myc*-pSG5 and R1a-*myc*-*PRDX3*AS cells. (Bar = 1 μM.) (*C*) Analysis of ROS after glucose deprivation. Cells were exposed to glucose-free media for 1.5 h before incubation with DCFH-DA.

glucose deprivation for 24 h. Cells that overexpress *PRDX3* show a reproducible increase in apoptosis, whereas cells with diminished *PRDX3* are resistant to apoptosis (Fig. 3*C*). These results confirm that *PRDX3* is required for proliferation in transformed cells, and that AS *PRDX3* inhibits apoptosis after glucose deprivation.

Effect of *PRDX3* on Mitochondrial Function and Structure. Because PRDX3 localizes to mitochondria, we examined several parameters that reflect mitochondrial integrity and function. Fig. 4*A* demonstrates that MCF7/ADR cells expressing *PRDX3*AS show increased levels of reactive oxygen species as measured by the redox-sensitive dye DCFH-DA (26), which is oxidized to fluorescent DCF. However, R1a-*myc*-*PRDX3*AS cells show a minimal increase in reactive oxygen species. Analysis of mitochondrial mass with 10-*N*-nonyl-acridine orange (NAO) (27) reveals that MCF7/ADR-*PRDX3*AS cells show decreased mitochondrial mass, whereas R1a-*myc*-*PRDX3*AS cells also show a small percentage of cells with reduced mitochondrial mass. Reduction of *PRDX3* in both cell lines results in a decrease in mitochondrial membrane potential, indicated by the reduced uptake of 3,3′-dihexyloxacarbocyanine iodide (DiOC$_6$), as shown in Fig. 4*A*. Although *PRDX3*AS cells have a lower mitochondrial mass and would, therefore, be expected to show reduced uptake of DiOC$_6$, the membrane potential is diminished even after the mitochondrial mass is taken into account (data not shown). In addition to functional defects, we also observed severe morphological defects when using electron microscopy. R1a-*myc*-*PRDX3*AS cells show distorted mitochondrial architecture, with elongated mi-

tochondria displaying branched or circular lobes (Fig. 4*B*). Analysis of 10 individual R1a-*myc*-pSG5 cells indicates that although some cells also had longer mitochondria, none of the cells showed branched or looped mitochondria. In contrast, 9 of 10 R1a-*myc*-*PRDX3*AS cells showed branched mitochondria, and 3 of 9 also showed looped mitochondria.

We hypothesized that the reduced mitochondrial membrane potential could prevent the generation of reactive oxygen species (ROS) during glucose deprivation-induced apoptosis. Previously, it had been shown that the mitochondrial membrane potential is required for generating ROS in bovine aortic endothelial cells after exposure to hyperglycemia (28). Analysis of MCF7/ADR cells after glucose withdrawal demonstrates that *PRDX3*AS cells show a minimal increase in ROS, whereas control cells show a dramatic increase in ROS (Fig. 4*C*).

Discussion

Our data suggest that one of the primary defects in *PRDX3*AS cells is a reduced mitochondrial membrane potential. The reduction in membrane potential may be a result of oxidative damage to components of the respiratory chain complexes (29), which, in turn, would disrupt the proton gradient across the inner mitochondrial membrane. A recent report attributing peroxynitrite reductase activity to bacterial peroxiredoxins (30) suggests peroxynitrite as a possible mediator of inhibition of respiratory chain activity and reduction of mitochondrial membrane potential (31). Our results are consistent with the observation that reduced levels of another mitochondrial antioxidant, MnSOD,

BIOCHEMISTRY

also result in mitochondrial dysfunction and reduced mitochondrial membrane potential (32).

Several reports underscore the potential significance of nuclear c-Myc target genes whose protein products localize to mitochondria. In one case, the mycER system was used to analyze thousands of genes on microarrays (4). Three genes with protein products that localize to mitochondria, peptidyl-prolyl *cis-trans* isomerase F, heat shock protein 60, and the chaperone grpE were identified by using this technique. Another study focused on genes regulated by *myc*-induced lymphomagenesis in the bursa of Fabricius (33). Several mitochondrial genes, including matrix nucleoside diphosphate kinase and matrix protein P1, were identified. Additionally, recent evidence suggests that the response of Myc to diverse apoptotic stimuli converges at a common mitochondrial signaling element (34).

Microarray analysis comparing c-*myc*$^{+/+}$ and c-*myc*$^{-/-}$ cells supports our conclusion that *PRDX3* is a c-Myc target gene (3). Rat *PRDX3*, termed thioredoxin peroxidase, was identified as a gene that was more highly expressed in both wild-type fibroblasts and *myc*$^{-/-}$ fibroblasts with reconstituted c-*myc* as compared with c-*myc*$^{-/-}$ cells. This same study also found that *PRDX3* expression was increased 2.4-fold upon expression of ectopic *myc* in normal c-*myc*$^{+/+}$ fibroblasts. This finding indicates that deregulated overexpression of *myc*, which mimics conditions found in cancer cells, induces *PRDX3*, and it suggests that at least some of the target genes that are regulated by *myc* under physiological conditions are also activated when *myc* is overexpressed. We hypothesize that Myc is not the sole regulator of *PRDX3* expression, as *PRDX3* is still expressed in *myc*$^{-/-}$ fibroblasts. Rather, *PRDX3* likely belongs to a class of genes that facilitates accelerated cellular growth and metabolism induced by c-Myc.

The mechanism by which c-Myc regulates both proliferation and apoptosis remains unclear. The c-Myc target gene ODC has been found to affect both processes, in that overexpression stimulates apoptosis, whereas inhibiting ODC activity blocks cell-cycle progression (35). This observation led to the multiple-effector model, whereby c-Myc regulates targets that overlap in function. In support of this model, our data indicate that Myc regulates a mitochondrial peroxiredoxin that is required for proliferation as well as apoptosis in transformed cells. Additionally, our results suggest that reduced mitochondrial function affects Myc-mediated transformation. Although is has been reported that the loss of mitochondrial membrane potential is a downstream event in Myc-mediated apoptosis (36), it is not known how the mitochondrial membrane potential affects proliferation and the apoptotic signaling cascade. Recently, it has been suggested that the mitochondrial membrane potential could be an integrator of growth, maturation, and apoptotic pathways (37). The observation that both transformation and apoptosis are affected in *PRDX3*AS cells supports this hypothesis.

1. Henriksson, M. & Luscher, B. (1996) *Adv. Cancer Res.* **68,** 109–182.
2. Schuhmacher, M., Kohlhuber, F., Holzel, M., Kaiser, C., Burtscher, H., Jarsch, M., Bornkamm, G. W., Laux, G., Polack, A., Weidle, U. H. & Eick, D. (2001) *Nucleic Acids Res.* **29,** 397–406.
3. Guo, Q. M., Malek, R. L., Kim, S., Chiao, C., He, M., Ruffy, M., Sanka, K., Lee, N. H., Dang, C. V. & Liu, E. T. (2000) *Cancer Res.* **60,** 5922–5928.
4. Coller, H. A., Grandori, C., Tamayo, P., Colbert, T., Lander, E. S., Eisenman, R. N. & Golub, T. R. (2000) *Proc. Natl. Acad. Sci. USA* **97,** 3260–3265.
5. Lewis, B. C., Shim, H., Li, Q., Wu, C. S., Lee, L. A., Maity, A. & Dang, C. V. (1997) *Mol. Cell. Biol.* **17,** 4967–4978.
6. Yamamoto, T., Matsui, Y., Natori, S. & Obinata, M. (1989) *Gene* **80,** 337–343.
7. Tsuji, K., Copeland, N. G., Jenkins, N. A. & Obinata, M. (1995) *Biochem. J.* **307,** 377–381.
8. Chae, H. Z., Chung, S. J. & Rhee, S. G. (1994) *J. Biol. Chem.* **269,** 27670–27678.
9. Kang, S. W., Chae, H. Z., Seo, M. S., Kim, K., Baines, I. C. & Rhee, S. G. (1998) *J. Biol. Chem.* **273,** 6297–6302.
10. Prosperi, M. T., Ferbus, D., Karczinski, I. & Goubin, G. (1993) *J. Biol. Chem.* **268,** 11050–11056.
11. Zhang, P., Liu, B., Kang, S. W., Seo, M. S., Rhee, S. G. & Obeid, L. M. (1997) *J. Biol. Chem.* **272,** 30615–30618.
12. Araki, M., Nanri, H., Ejima, K., Murasato, Y., Fujiwara, T., Nakashima, Y. & Ikeda, M. (1999) *J. Biol. Chem.* **274,** 2271–2278.
13. Noh, D. Y., Ahn, S. J., Lee, R. A., Kim, S. W., Park, I. A. & Chae, H. Z. (2001) *Anticancer Res.* **21,** 2085–2090.
14. Eilers, M., Picard, D., Yamamoto, K. R. & Bishop, J. M. (1989) *Nature (London)* **340,** 66–68.
15. Stone, J., de Lange, T., Ramsay, G., Jakobovits, E., Bishop, J. M., Varmus, H. & Lee, W. (1987) *Mol. Cell. Biol.* **7,** 1697–1709.
16. Evan, G. I., Wyllie, A. H., Gilbert, C. S., Littlewood, T. D., Land, H., Brooks, M., Waters, C. M., Penn, L. Z. & Hancock, D. C. (1992) *Cell* **69,** 119–128.
17. Shim, H., Chun, Y. S., Lewis, B. C. & Dang, C. V. (1998) *Proc. Natl. Acad. Sci. USA* **95,** 1511–1516.
18. Fairchild, C. R., Ivy, S. P., Kao-Shan, C. S., Whang-Peng, J., Rosen, N., Israel, M. A., Melera, P. W., Cowan, K. H. & Goldsmith, M. E. (1987) *Cancer Res.* **47,** 5141–5148.
19. Kim, S., Li, Q., Dang, C. V. & Lee, L. A. (2000) *Proc. Natl. Acad. Sci. USA* **97,** 11198–11202.
20. Boyd, K. E., Wells, J., Gutman, J., Bartley, S. M. & Farnham, P. J. (1998) *Proc. Natl. Acad. Sci. USA* **95,** 13887–13892.
21. Egan, S. E., Giddings, B. W., Brooks, M. W., Buday, L., Sizeland, A. M. & Weinberg, R. A. (1993) *Nature (London)* **363,** 45–51.
22. Littlewood, T. D., Hancock, D. C., Danielian, P. S., Parker, M. G. & Evan, G. I. (1995) *Nucleic Acids Res.* **23,** 1686–1690.
23. Mateyak, M. K., Obaya, A. J., Adachi, S. & Sedivy, J. M. (1997) *Cell. Growth Differ.* **8,** 1039–1048.
24. Lee, Y. J., Galoforo, S. S., Berns, C. M., Tong, W. P., Kim, H. R. & Corry, P. M. (1997) *J. Cell Sci.* **110,** 681–686.
25. Lee, Y. J., Galoforo, S. S., Berns, C. M., Chen, J. C., Davis, B. H., Sim, J. E., Corry, P. M. & Spitz, D. R. (1998) *J. Biol. Chem.* **273,** 5294–5299.
26. Hockenbery, D. M., Oltvai, Z. N., Yin, X. M., Milliman, C. L. & Korsmeyer, S. J. (1993) *Cell* **75,** 241–251.
27. Petit, J. M., Maftah, A., Ratinaud, M. H. & Julien, R. (1992) *Eur. J. Biochem.* **209,** 267–273.
28. Nishikawa, T., Edelstein, D., Du, X. L., Yamagishi, S., Matsumura, T., Kaneda, Y., Yorek, M. A., Beebe, D., Oates, P. J., Hammes, H. P., *et al.* (2000) *Nature (London)* **404,** 787–790.
29. Zhang, Y., Marcillat, O., Giulivi, C., Ernster, L. & Davies, K. J. (1990) *J. Biol. Chem.* **265,** 16330–16336.
30. Bryk, R., Griffin, P. & Nathan, C. (2000) *Nature (London)* **407,** 211–215.
31. Brown, G. C. (1999) *Biochim. Biophys. Acta* **1411,** 351–369.
32. Kokoszka, J. E., Coskun, P., Esposito, L. A. & Wallace, D. C. (2001) *Proc. Natl. Acad. Sci. USA* **98,** 2278–2283.
33. Neiman, P. E., Ruddell, A., Jasoni, C., Loring, G., Thomas, S. J., Brandvold, K. A., Lee, R., Burnside, J. & Delrow, J. (2001) *Proc. Natl. Acad. Sci. USA* **98,** 6378–6383.
34. Soucie, E. L., Annis, M. G., Sedivy, J., Filmus, J., Leber, B., Andrews, D. W. & Penn, L. Z. (2001) *Mol. Cell. Biol.* **21,** 4725–4736.
35. Packham, G., Porter, C. W. & Cleveland, J. L. (1996) *Oncogene* **13,** 461–469.
36. Hotti, A., Jarvinen, K., Siivola, P. & Holtta, E. (2000) *Oncogene* **19,** 2354–2362.
37. Augenlicht, L. H. & Heerdt, B. G. (2001) *Nat. Genet.* **28,** 104–105.
38. Grandori, C., Mac, J., Siebelt, F., Ayer, D. E. & Eisenman, R. N. (1996) *EMBO J.* **15,** 4344–4357.
39. Blackwell, T. K., Huang, J., Ma, A., Kretzner, L., Alt, F. W., Eisenman, R. N. & Weintraub, H. (1993) *Mol. Cell. Biol.* **13,** 5216–5224.